Engineering the magnetism of nanographene via co-depositing hetero precursors

Hui Zhang
Kunming University of Science and Technology
Jianchen Lu
Kunming University of Science and Technology
Yong Zhang
Kunming University of Science and Technology
Lei Gao
Institute of Physics & University of Chinese Academy of Sciences, Chinese Academy of Sciences
Xin-Jing Zhao
College of Chemistry and Chemical Engineering, Xiamen University
Yuan-Zhi Tan
College of Chemistry and Chemical Engineering, Xiamen University https://orcid.org/0000-0002-1268-2761
Jinming Cai (j.cai@kust.edu.cn)
Kunming University of Science and Technology

Article

Keywords: nanographene, magentism, carbon nanomaterials

Posted Date: June 23rd, 2021

DOI: https://doi.org/10.21203/rs.3.rs-595946/v1

Engineering the magnetism of nanographene via co-depositing hetero precursors

Hui Zhang [1]*, Jiancheng Lu [1]*, Yong Zhang [1], Lei Gao [2], Xin-Jing Zhao[3], Yuan-Zhi Tan [3]✉, Jinming Cai [1]✉

[1] Faculty of Materials Science and Engineering, Kunming University of Science and Technology, No. 68 Wenchang Road, Kunming 650093, China.

[2] Faculty of Science, Kunming University of Science and Technology, No. 727 Jingming South Road, Kunming 650500, China.

[3] State Key Laboratory for Physical Chemistry of Solid Surfaces, Collaborative Innovation Center of Chemistry for Energy Materials, and Department of Chemistry, College of Chemistry and Chemical Engineering, Xiamen University, Xiamen 361005, China.

* These authors contributed equally to this work.

✉ Email: yuanzhi_tan@xmu.edu.cn; j.cai@kust.edu.cn.

Abstract

The magnetism of carbon nanomaterials is dominated by the structure of its carbon skeleton. However, the magnetism engineering is hindered due to finite precursors. Here, we develop a new strategy to engineer the magnetism of nanographene through hetero-coupling two different precursors on Au (111) surface by using low-temperature bond-resolved scanning tunneling microscopy and scanning tunneling spectroscopy, combined with spin-polarized density functional theory calculations. Our results demonstrate that two homo-coupled products host close shell structure along with defects inducing magnetic one with the total spin number S = 1/2. Upon simultaneous depositing with another precursor, two hetero-coupled products switch to magnetic structure with the S = 1/2 and S = 1 resulting from carbon skeleton transformation. Our results provide a valid way via inducing different molecular precursors to engineer the magnetism of carbon nanomaterials, which could be extended in other magnetic materials instruction.

Introduction

The magnetism of carbon nanomaterials, such as nanographene (NG), has been triggering much attention due to its high magnitudes of spin-wave stiffness[1], weak spin-orbit coupling[2], hyperfine couplings[3] and large spin coherence lifetimes[4], which hold promise for high temperature magnets, spin-polarized current transports[5], and spin-based quantum information processing[2, 6-9]. The open-shell[10, 11] structure of magnetic NGs with high reactivity is resulted from the presence of unpair electrons (radicals), which makes it challenging in solution-based synthesis and magnetic ground state measurement[12, 13]. However, as an alternative method, on surface synthesis under ultra-high vacuum has emerged as a powerful flexible synthetic toolkit in recent years[14, 15]. The current issues of carbon magnetism involve around three aspects: NG or graphene nanoribbons (GNR) with spin-polarized zigzag edges states[16-19], sublattice imbalance as guided by Lerb's theorem for bipartite latices[20-24] and NGs with non-Kekulé structure which is formed via Coulomb repulsion between valence electrons[25-32].

The total spin quantum number (S) of NGs might be engineered in three ways. Firstly, the radical positions of NGs could be passivated by H atoms released from cyclodehydrogenation, which will modulate S from 0 to 1/2[28] and 1 to 1/2[23]. In this situation, the S could be recovered by applying bias to remove the redundant H atoms. Secondly, quenching the spin by creating single C–metal bond, for example, bounding the radical positions to the elbow area of Au(111) surface[28] by applying positive voltage pulse[33]. Thirdly, the spin on/off could be switched due to the charge transfer by changing adsorption positions[34-36]. The aspects mentioned above can be considered as the tip manipulation of spin. However, the direct structural engineering of products processes more possibilities to switch the magnetisms.

Originally, here we inducing co-deposition method in magnetism engineering from structural level and proved to be an effective method. By co-depositing two different precursors (precursor **1**, 9-bromo-10-(2,6-dimethylphenyl) anthracene, **BDMPA**[31]; precursor **2**, 10-bromo-9,9'-bianthracene, **BBA**[37]) on Au(111).

Bond-resolved scanning tunneling microscope (BR-STM), scanning tunneling spectroscopy (STS), together with spin-polarized density functional theory (SP-DFT) calculations are combined to determine the atomic structures, electronic, and magnetic properties of two homo-coupled products and two hetero-coupled products.

Design synthesis routes of magnetic NGs. As illustrated in route 1 of figure 1, surface-catalyzed Ullmann homo-coupling and afterwards cyclodehydrogenation reactions (300 °C, 6 °C/min) of precursor **1** lead to the formation of NG **1a** (defect-free). Simultaneously, the NG **1b** endowed with a pentagonal terminus resulting from losing a methyl group in precursor **1** could be formed as well during the annealing process. According to chemical structures and Lerb's theorem[24], the total spin of **1a** and **1b** is 0 and 1/2, respectively. NG **1a** can be described as either an open shell non-Kekulé structure with 5 Clar sextets or a close shell Kekulé structure with 4 Clar sextets, respectively. The aromaticity of 5 Clar sextets is higher than 4 Clar sextets one, resulting in the higher kinetically stability[38], whereas the open shell structure is more reactive than the close shell. In addition, DFT calculation show that the real structure of NG **1a** is still ambiguous (Supplementary table 1) as the energies of open shell and close shell structures are almost the same. When missing a methyl group in precursor **1**, a pentagonal topological defect in NG **1b** raises a result of sublattice-imbalance, which manifests as a Kondo resonance. In another synthesis routes (route **2**), surface-catalyzed Ullmann hetero-coupling of precursor **1** and precursor **2** and afterwards cyclodehydrogenation cyclization reactions (300 °C, 6 °C/min) lead to the formations of NG **2a** and NG **2b**. NG **2a**, a defect-free structure, possesses a triplet ground state (S = 1). NG **2b**, similar with NG **1b**, formed by missing a methyl group**,** has a doublet ground state (S = 1/2). The radical positions of NG **2a** is still ambiguous[16, 23], even though a 6 Clar sextets structure is energetically preferred (Supplementary fig. 5).

On-surface synthesis of magnetic NGs and their electronic and magnetic characterizations. After depositing the precursor **1** on Au(111) surface and

subsequent cyclodehydrogenation, the NG **1a** and **1b** was obtained (figure 2). Figure 2a and figure 2b show the chemical structures of NG **1a** and **1b,** respectively, where red and blue balls represent carbon atoms of different sublattices. The NG **1a** can be clearly recognized from the STM image via the two-lobe-like feature at both triangular termini, while the NG **1b** possesses such feature at only one of the triangular ends (figure 2c). To elucidate the experimental electronic properties, we employ STS characterizations of NG **1a** (figure 2e) and **1b** (figure 2f). For NG **1a**, the STS depicts several electronic resonances labeled as HOMO-1 (–1.35 V), LUMO+1 (+2.0 V) and a pair of electronic resonances marked as frontier molecular orbitals. The absence of any spin enhanced state near fermi level from BR-STM (Supplementary table 1) and inelastic spin excitation signal in higher-energy resolution dI/dV spectroscopy (Supplementary fig.1) which may illustrate a close shell structure of NG 1a. The precise energy positions of LOMO and HUMO are identified to be –0.3 V and +0.21 V, respectively, which reveals a frontier gap of 0.51 eV for NG **1a**. The spatial maps of electronic state distribution of HOMO-1 (figure 2g), and LUMO+1 (figure 2h) reveal similar results as reported before[22]. For NG **1b**, the STS mainly shows two electronic resonances, labeled as HOMO-1 (–1.1 V) and LUMO+1 (+1.6 V). The sublattice imbalanced non-Kekulé NG **1b** (S = 1/2) displays a two-lobe like feature at one terminus (figure 2d). Figure 2i, figure 2j and Supplementary fig. 2 show the spatial maps of electronic states distribution of HOMO-1 and LUMO+1. dI/dV spectra in figure 2f depict the zero-energy states (ZESs) near the defect free terminus (the purple and green lines in figure 2f). To amplify on the ZES of NG 1b, we performed low-energy range dI/dV spectra in Supplementary fig. 3. The ZES appears when the tip position is close to defect free area and the resonance fits well with the Frota function[39]. These results mean that the ZES in NG **1b** is attributed to the Kondo resonances[20-23, 40, 41].

To engineer the NG magnetism, we co-deposited the precursor **1** and precursor **2** onto Au(111) substrate. After annealing process, two new products (NG **2a** and **2b**) were observed, as shown in figure 3a. NG **2a** and **2b** are marked by solid white rectangles (figure 3a). The difference between NG **2a** and **2b** can be distinguished

from the zoom-in highly-resolved STM images (figure 3b and figure 3c). The two-lobe like local density states distribution shown in figure 3b corresponds to the triangular end of NG **2a**, while the pentagonal defect terminus of NG **2b** shows a faint feature (figure 3c). To gain bond-resolved images of NG **2a** and **2b**, we performed ultra-high resolution STM characterizations by attaching a CO molecule at the apex of tip. Figure 3d and figure 3e depict bond-resolved STM (BR-STM) images of NG **2a** and **2b**, respectively, confirming the defect-free feature of NG **2a** and pentagonal defect feature of NG **2b**. Both BR-STM images show non-planar features, indicating the Kondo resonance enhanced state distributions[22, 23]. Moreover, BR-STM image for NG **2a** shows the non-planar feature around the whole structure, while only the bottom part of NG **2b** BR-STM image shows the non-planar feature. The difference means that the Kondo resonance distributions of NG **2a** and NG **2b**. dI/dV spectra of NG **2a** and **2b** shown in figure 3f and figure 3g shed light on the energy positions of HOMO-1 and LUMO+1. Moreover, the ZESs are also observed at the dI/dV spectra of the positions chosen in figure 3b and figure 3c. The distributions of ZESs for NG **2a** and **2b** fit well with the electronic-state enhanced area of BR-STM images in figure 3d and figure 3e. dI/dV maps at –1.3 V, and +1.7 V for NG 2a (figure 3h,i) and –1.0 V, and +1.4 V for NG **2b** (figure 3j,k) reveal spatial maps of electronic states.

SP-DFT calculated the magnetism of NG 2a and 2b. To further illuminate the electronic structures and magnetic properties of NG **2a** and **2b**, we performed SP-DFT calculations. Figure 4a and figure 4b present the SP-DFT calculated energy spectra of NG **2a** and **2b**, which show the single electron occupied frontier orbitals SOMOs and SUMOs of the degenerated energy level ψ_2 and ψ_3 of NG **2a** and the energy level ψ_2 of NG **2b** respectively, triggering spin polarizations. According to calculated energy level, the magnetic ground states of NG **2a** and **2b** are S = 1 and S = 1/2 respectively. The computed spin-polarized wave functions of the SOMOs of NG **2a** and **2b** are displayed in Figures 4c and 4d, respectively. $\psi_{2\uparrow}$ and $\psi_{3\uparrow}$ of the NG **2a**

exhibit dominant localization at the top and bottom terminus respectively. $\psi_{2\uparrow}$ of the NG **2b** only exhibit dominant localization at the bottom area. The spin density distribution of the triplet ground state NG **2a** shown in figure 4e is around the whole C_B atoms, while the doublet ground state NG **2b** in figure 4f is around at the bottom C_B atoms of the NG **2b**. Furthermore, the calculated spin density layouts fit well with experimental BR-STM results (figure 3d and figure 3e). Low-energy interval dI/dV spectra at the marked positions (figure 4g and figure 4h) reveal the existence of Kondo resonances. The distributions of Kondo resonance fit well with the calculate spin density state distributed area. The Kondo peak positions are slight away from fermi level and the shapes are slight asymmetric which can be attributed to the charge transfer from substrate and the hybridization with the substate[34, 35, 42]. In contrast to the S = 0 ground state structure of homo-coupled NG **1a**, the ground state of NG **2a,** formed by hetero-coupling of two different precursors**,** is switched to triplet. A detailed comparison of homo-coupled NG **1a** and hetero-coupled NG **2a** is summarized, as shown in Supplementary table 2, confirming the magnetism engineering.

Conclusion

In the final analysis, we demonstrate a new strategy to engineer the magnetism of NGs by using combined bond-resolved scanning tunneling microscopy, scanning tunneling spectroscopy as well as spin-polarized density functional theory. Two homo-coupled products (NG **1a** and NG **1b**) acquired by Ullmann coupling and cyclodehydrogenation reactions of precursor **1** and two hetero-coupled products (NG **2a** and NG **2b**) co-deposited by precursor **1** and precursor **2** have been successively fabricated. Even though the calculated energy of open shell structure and the close shell one is comparable, the defect-free NG **1a** performs as the non-magnetic close shell structure as no enhanced state and inelastic spin excitation signal was detected. Defective NG **1b** host spins of S = 1/2 resulting from a sublattice imbalanced carbon skeleton. Co-deposition induced magnetism switching for defect-free NG **2a** and

defective NG **2b** host spins of S = 1/2 and S = 1, respectively. Our work successfully realizes the magnetism engineering by inducing another precursor and offers a valid opportunity via the co-deposition to extend the magnetism engineering of NG on metal substrate.

Methods

1. Sample/tip preparation and STM/STS measurements

All the STM measurements were operated with a commercial LT-STM from Scienta Omicron under ultra-high vacuum (base pressure better than 1 x 10^{-10} mbar) at a temperature of 4.2 K. Au(111) single crystal was prepared with several cycles Ar^+ ions sputtering and following annealing at 800 K. Precursor **1** and **2** were deposited at 348 K and 318 K from a commercial 4-cell evaporator on clean Au(111) held at 453K, respectively and post-annealing at 573 K for cyclodehydrogenation and oxidative cyclization (6 °C/min). A tungsten tip was fabricated via electrochemical corrosion. To fabricate gold decorated tungsten tip for the STM imaging and spectroscopy, tungsten tip was slightly indent to the Au(111) single crystal. All STM and STS measurements were performed in constant current mode, except for noting otherwise. The tunneling bias voltages are applied with respect to the sample. dI/dV spectra and maps were obtained with a lock-in amplifier (Zurich Instruments) operating at a frequency of 600 Hz. Lock-in modulation voltages (V_{rms}) are given in the figure captions. Bond resolving STM images were acquired in constant-height mode with a CO-functionalized tip, and the current signal was recorded. The preparation of CO-functionalized tips is prepared as the papers guided before[43]. The data were processed and analyzed with WSxM software[44].

2. Spin-polarized density functional theory calculations

Spin-polarized density functional theory (DFT) calculations were performed using the Vienna ab-initio simulation package (VASP)[45, 46]. A generalized gradient approximation (GGA) in the form of Perdew-Burke-Ernzerhof (PBE)[47] used for the

exchange and correlation functional. H atoms were included to saturate dangling bonds. The electronic wavefunctions are expanded in a plane wave basis with an energy cutoff of 600 eV. In all the calculations, 15 Å vacuum layers in all three directions are used, and all atoms are fully relaxed until the residual forces on each atom are smaller than 0.01 eV/Å.

Data availability

The authors declare that all the relevant data of this study are available.

References

1. Edwards, D. M., Katsnelson, M. I. High-temperature ferromagnetism of sp electrons in narrow impurity bands: application to CaB6. *J. Phys. Condens. Matter* **18**, 7209-7225 (2006).
2. Yazyev, O. V. Emergence of magnetism in graphene materials and nanostructures. *Rep. Prog. Phys.* **73**, 056501 (2010).
3. Trauzettel, B., Bulaev, D. V., Loss, D., Burkard, G. Spin qubits in graphene quantum dots. *Nat. Phys.* **3**, 192-196 (2007).
4. Yazyev, O. V., Katsnelson, M. I. Magnetic correlations at graphene edges: basis for novel spintronics devices. *Phys. Rev. Lett.* **100**, 047209 (2008).
5. Son, Y. W., Cohen, M. L., Louie, S. G. Half-metallic graphene nanoribbons. *Nature* **444**, 347-349 (2006).
6. Atzori, M., Tesi, L., Morra, E., Chiesa, M., Sorace, L., Sessoli, R. Room-Temperature Quantum Coherence and Rabi Oscillations in Vanadyl Phthalocyanine: Toward Multifunctional Molecular Spin Qubits. *J. Am. Chem. Soc.* **138**, 2154-2157 (2016).
7. Bader, K. *et al.* Room temperature quantum coherence in a potential molecular qubit. *Nat. Commun.* **5**, 1-5 (2014).
8. Han, W., Kawakami, R. K., Gmitra, M., Fabian, J. Graphene spintronics. *Nat. Nanotechnol.* **9**, 794-807 (2014).
9. Warner, M. *et al.* Potential for spin-based information processing in a thin-film molecular semiconductor. *Nature* **503**, 504-508 (2013).
10. Morita, Y., Suzuki, S., Sato, K., Takui, T. Synthetic organic spin chemistry for structurally well-defined open-shell graphene fragments. *Nat. Chem.* **3**, 197-204 (2011).
11. Zeng, W., Wu, J. Open-Shell Graphene Fragments. *Chem* **7**, 358-386 (2021).
12. Small, D., Zaitsev, V., Jung, Y., Rosokha, S. V., Head-Gordon, M., Kochi, J. K. Intermolecular π-to-π Bonding between Stacked Aromatic Dyads. Experimental and Theoretical Binding Energies and Near-IR Optical Transitions for Phenalenyl Radical/Radical versus Radical/Cation Dimerizations. *J. Am. Chem. Soc.* **126**, 13850-13858 (2004).
13. Goto, K. *et al.* A Stable Neutral Hydrocarbon Radical: Synthesis, Crystal Structure, and Physical Properties of 2,5,8-Tri-tert-butyl-phenalenyl. *J. Am. Chem. Soc.* **121**, 1619-1620 (1999).

14. On-Surface Synthesis; Gourdon, A., Ed.; Springer International Publishing: Cham, 2016
15. Cai, J. *et al.* Atomically precise bottom-up fabrication of graphene nanoribbons. *Nature* **466**, 470-473 (2010).
16. Li, J. *et al.* Single spin localization and manipulation in graphene open-shell nanostructures. *Nat. Commun.* **10**, 1-10 (2019).
17. Jung, J., MacDonald, A. H. Carrier density and magnetism in graphene zigzag nanoribbons. *Phys. Rev. B* **81**, 235433 (2009).
18. Nakada, K., Fujita, M., Dresselhaus, G., Dresselhaus, M. S. Edge state in graphene ribbons: Nanometer size effect and edge shape dependence. *Phys. Rev. B* **54**, 17954-17961 (1996).
19. Fernandez-Rossier, J., Palacios, J. J. Magnetism in graphene nanoislands. *Phys. Rev. Lett.* **99**, 177204 (2007).
20. Pavlicek, N. *et al.* Synthesis and characterization of triangulene. *Nat. Nanotechnol.* **12**, 308-311 (2017).
21. Mishra, S. *et al.* Synthesis and Characterization of pi-Extended Triangulene. *J. Am. Chem. Soc.* **141**, 10621-10625 (2019).
22. Mishra, S. *et al.* Topological Defect-Induced Magnetism in a Nanographene. *J. Am. Chem. Soc.* **142**, 1147-1152 (2020).
23. Li, J. *et al.* Uncovering the Triplet Ground State of Triangular Graphene Nanoflakes Engineered with Atomic Precision on a Metal Surface. *Phys. Rev. Lett.* **124**, 177201 (2020).
24. Lieb, E. H. Two theorems on the Hubbard model. *Phys. Rev. Lett.* **62**, 1201-1204 (1989).
25. Sanchez-Grande, A. *et al.* Diradical Organic One-Dimensional Polymers Synthesized on a Metallic Surface. *Angew. Chem. Int. Ed.* **59**, 17594-17599 (2020).
26. Mishra, S. *et al.* Giant magnetic exchange coupling in rhombus-shaped nanographenes with zigzag periphery. Preprint at https://ui.adsabs.harvard.edu/abs/2020arXiv200303577M (2020).
27. Mishra, S. *et al.* On-surface synthesis of super-heptazethrene. *Chem. Commun.* **56**, 7467-7470 (2020).
28. Mishra, S. *et al.* Topological frustration induces unconventional magnetism in a nanographene. *Nat. Nanotechnol.* **15**, 22-28 (2020).
29. Mishra, S. *et al.* Collective All-Carbon Magnetism in Triangulene Dimers. *Angew. Chem. Int. Ed.* **59**, 12041-12047 (2020).
30. Wang, W. L., Yazyev, O. V., Meng, S., Kaxiras, E. Topological Frustration in Graphene Nanoflakes: Magnetic Order and Spin Logic Devices. *Phys. Rev. Lett.* **102**, 157201 (2009).
31. Mishra, S. *et al.* Large magnetic exchange coupling in rhombus-shaped nanographenes with zigzag periphery. *Nat. Chem.* (2021).
32. Mishra, S. *et al.* Tailoring Bond Topologies in Open-Shell Graphene Nanostructures. *ACS Nano* **12**, 11917-11927 (2018).
33. van der Lit, J. *et al.* Suppression of electron-vibron coupling in graphene nanoribbons contacted via a single atom. *Nat. Commun.* **4**, 1-6 (2013).
34. Zhao, Y. *et al.* Precise Control of pi-Electron Magnetism in Metal-Free Porphyrins. *J. Am. Chem. Soc.* **142**, 18532-18540 (2020).
35. Sun, Q. *et al.* Inducing Open-Shell Character in Porphyrins through Surface-Assisted Phenalenyl pi-Extension. *J. Am. Chem. Soc.* **142**, 18109-18117 (2020).
36. Kumar, A. *et al.* Charge-Transfer-Driven Nonplanar Adsorption of F4TCNQ Molecules on Epitaxial Graphene. *ACS Nano* **11**, 4960-4968 (2017).

37. Lee, H., Jo, M., Yang, G., Jung, H., Kang, S., Park, J. Highly efficient dual anthracene core derivatives through optimizing side groups for blue emission. *Dyes Pigm.* **146**, 27-36 (2017).
38. Sola, M. Forty years of Clar's aromatic pi-sextet rule. *Front Chem* **1**, 22 (2013).
39. Frota, H. O. Shape of the Kondo resonance. *Phys. Rev. B* **45**, 1096-1099 (1992).
40. Su, X., Li, C., Du, Q., Tao, K., Wang, S., Yu, P. Atomically Precise Synthesis and Characterization of Heptauthrene with Triplet Ground State. *Nano Lett.* **20**, 6859-6864 (2020).
41. Ternes, M., Heinrich, A. J., Schneider, W. D. Spectroscopic manifestations of the Kondo effect on single adatoms. *J. Phys. Condes. Matter* **21**, 053001 (2009).
42. Ternes, M. Spin excitations and correlations in scanning tunneling spectroscopy. *New J. Phys.* **17**, 063016 (2015).
43. Bartels, L. *et al.* Dynamics of Electron-Induced Manipulation of Individual CO Molecules on Cu(111). *Phys. Rev. Lett.* **80**, 2004-2007 (1998).
44. Horcas, I., Fernandez, R., Gomez-Rodriguez, J. M., Colchero, J., Gomez-Herrero, J., Baro, A. M. WSXM: a software for scanning probe microscopy and a tool for nanotechnology. *Rev. Sci. Instrum.* **78**, 013705 (2007).
45. Kresse, G., Furthmüller, J. Efficient iterative schemes for ab initio total-energy calculations using a plane-wave basis set. *Phys. Rev. B* **54**, 11169-11186 (1996).
46. Kresse, G., Furthmüller, J. Efficiency of ab-initio total energy calculations for metals and semiconductors using a plane-wave basis set. *Comput. Mater. Sci.* **6**, 15-50 (1996).
47. Perdew, J. P., Burke, K., Ernzerhof, M. Generalized Gradient Approximation Made Simple. *Phys. Rev. Lett.* **77**, 3865-3868 (1996).

Acknowledgements

We appreciate Dr. Can Li and Dr. Jingcheng Li for constructive assistances. This work was supported by the National Natural Science Foundation of China (Grant Nos. 61901200 and 12064020), the National Recruitment Program for Young Professionals (132310976002), the Yunnan Province Science and Technology Plan Project (Grant No. 2019FD041), the Strategic Priority Research Program of Chinese Academy of Sciences (XDB30010000), the Reserve Talents for Yunnan Young and Middle Aged Academic and Technical Leaders (2017HB010), the Yunnan Province for Recruiting High-Caliber Technological Talents (1097816002).

Author contributions

J.C. conceived the whole experiments, J.C., J.L., and Y.T. supervised the project, H. Z., Y.Z., prepared the samples and performed the STM/STS and experiments. L.G. performed the DFT calculations. H.Z. performed the data fitting. X.Z. and Y.T.

synthesized the molecular precursor. H.Z., J.L., and J.C., analyzed the data. H.Z., wrote the paper. All authors discussed the results and implications and commented on the manuscript at all stages.

Competing interests

The authors declare no competing interests.

Additional information

Supplementary information is available for this paper at

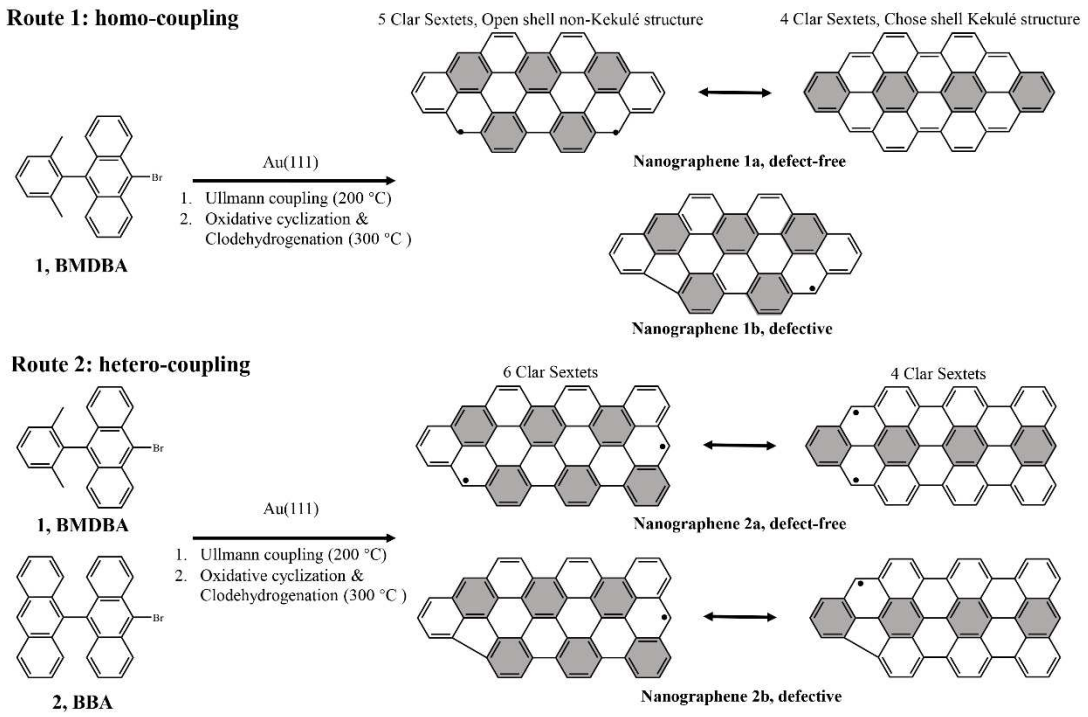

Figure 1 | Synthetic Routes toward NGs 1a, 1b, 2a and 2b. Route 1: precursor **1**, 9-bromo-10-(2,6-dimethylphenyl) anthracene (BDMPA), undergoes homo-coupling into the defect-free NG **1a** at Au(111) substrate. During the annealing process, the defective NG **1b** could be fabricated by missing a methyl group. Route 2: precursors **1** and **2** (10-bromo-9,9'-bianthracene, BBA) hetero-coupling into the defect-free NG **2a** at Au(111) substrate. Similar with NG 1b, the defective NG 2b could also be fabricated. The total spin of NG **1a** and **1b** in route 1 is 0 and 1/2 respectively and of NG **2a** and **2b** in route 2 is 1 and 1/2 respectively.

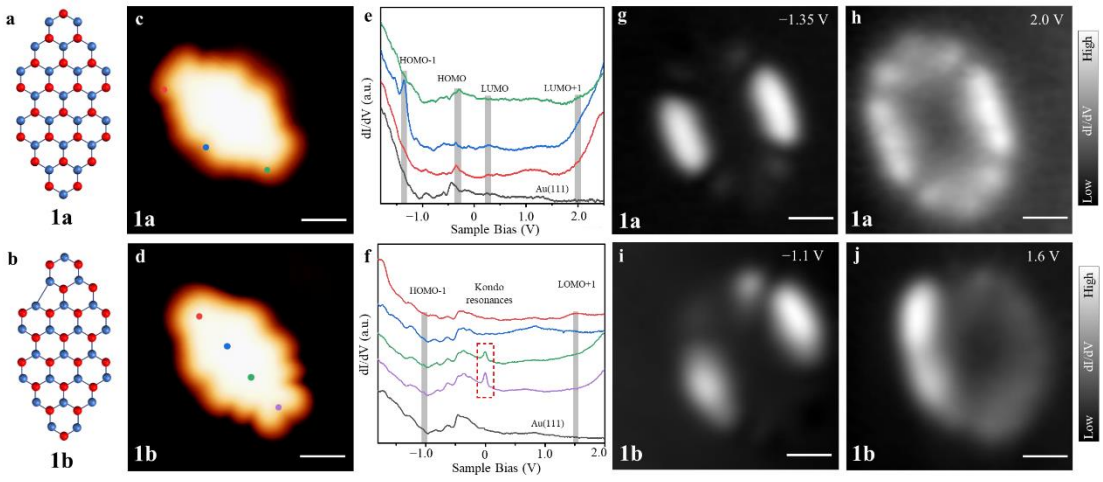

Figure 2 | STM images and electronic structures of NG 1a and 1b. (**a,b**) Chemical structures of bipartite NG **1a** and **1b**. The red and blue balls denote carbon atoms from two different sublattices. (**c,d**)

STM images of NG **1a** (**c**) and **1b** (**d**) on Au(111). Tunneling parameters: V = −500 mV, I = 200 pA. (**e,f**) dI/dV spectroscopy on NG **1a** (**e**) and **1b** (**f**). Signal acquisition positions are marked with corresponding to filled circles in (**c**) and (**d**). The orbital positions are marked by grey bars. The Kondo resonances are circled by a red dotted rectangle. Tunneling parameters: V = −2 V, I = 350 pA, V_{rms} = 15 mV. (**g,h**) Experimental dI/dV maps of HOMO-1 and LUMO+1 for NG **1a**. Tunneling parameters: V = –1.35 V, I = 350 pA (**g**, HOMO-1); V = +2.0 V, I = 350 pA (**h**, LUMO+1); V_{rms} = 15 mV. (**i,j**) Experimental dI/dV maps of HOMO−1 and LUMO+1 for NG **1b**. Tunneling parameters: V = –1.1 V, I = 350 pA (**i**, HOMO-1); V = +1.6V, I = 350 pA (**j**, LUMO+1); V_{rms} = 15 mV. Scale bar: 0.6 nm.

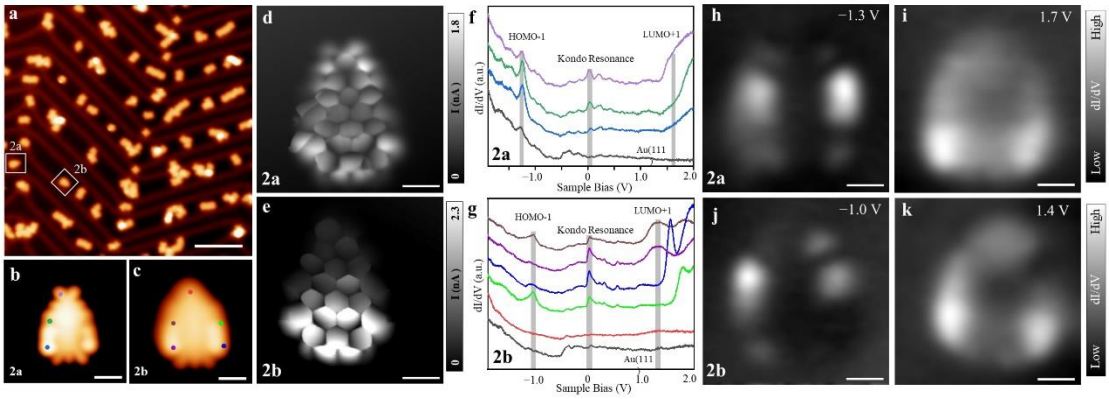

Figure 3 | STM images and electronic structures of NG 2a and 2b. (**a**) Large-scale STM image of NG **2a** and **2b** on Au(111). Tunneling parameters: V = −1 V, I = 30 pA. Scale bar: 10 nm. (**b,c**) High-resolution STM images of NG **2a** (**b**) and **2b** (**c**). Tunneling parameters: V = +2 mV, I = 200 pA. Scale bar: 0.6 nm. (**d,e**) BR-STM images with CO functionalized tip for NG **2a** (**d**) and **2b** (**e**). Tunneling parameters: V = +2 mV, Δz = 220 pm (**d**). V = +2 mV, Δz = 120 pm (**e**). Scale bar: 0.5 nm. (**f,g**) dI/dV spectra of NG **2a** (**f**) and **2b** (**g**). The signal acquisition positions are marked on the inset figures. Tunneling parameters: V = –2.0 V, I = 350 pA. (**h,i**) Experimental dI/dV maps of HOMO-1 and LUMO+1 of NG **2a**. Tunneling parameters: V = –1.3 V, I = 350 pA (**h**, HOMO-1); V = +1.7 V, I = 350 pA (**i**, LUMO+1). V_{rms} = 15 mV. Scale bar: 6 Å. (**j,k**) Experimental dI/dV maps of HOMO-1 and LUMO+1 of NG **2b**. Tunneling parameters: V = –1.0 V, I = 350 pA (**j**, HOMO-1); V = +1.4 V, I = 350 pA (**k**, LUMO+1). Scale bar: 0.6 nm.

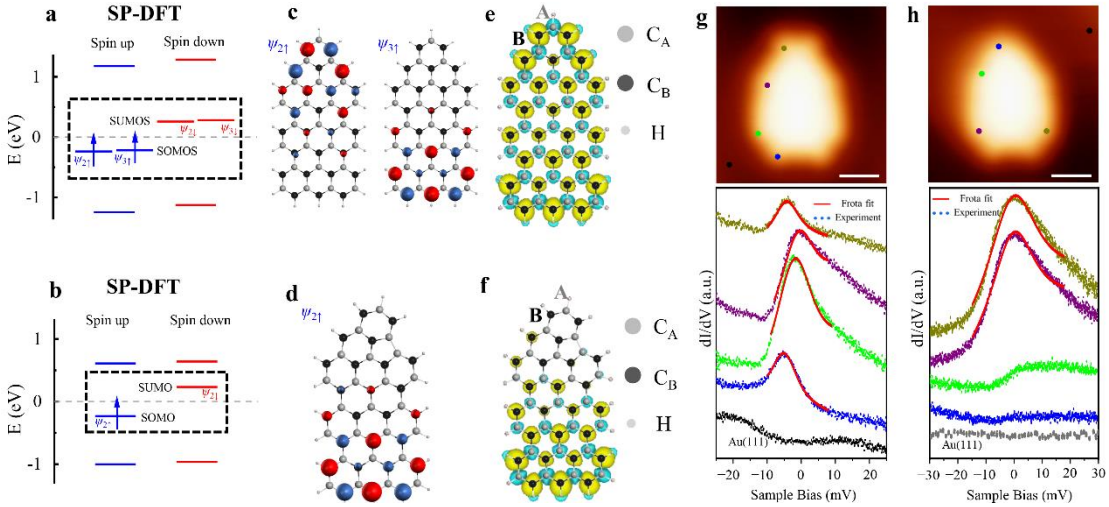

Figure 4 | SP-DFT calculated magnetic properties of NG 2a and 2b. (**a,b**) SP-DFT calculated energy spectra of NG **2a** and **2b**. (**c,d**) DFT calculated spin-polarized wave functions of the SOMO of NG **2a** (**c**) and **2b** (**d**). (**e,f**) SP-DFT simulated spin density distributions of NG **2a** (**e**) and **2b** (**f**). Grey and black balls represent carbon atoms from two different sublattice. The spin density marked by cyan and yellow represent two different spin directions. (**g,h**) Experimental low-energy ranges dI/dV spectra of the Kondo resonances detected in **2a** (g) and **2b** (**h**), with fitting using the Frota function[39].

Supplementary Files

This is a list of supplementary files associated with this preprint. Click to download.

- Supplementaryinformation.pdf